Report No.
UCB/SEMM-2011/05

Structural Engineering
Mechanics and Materials

RESPONSE OF TALL CANTILEVER WALL BUILDINGS TO STRONG PULSE TYPE SEISMIC EXCITATION

By

Vladimir Calugaru and Marios Panagiotou

July 2011

Department of Civil and Environmental Engineering
University of California, Berkeley

Response of Tall Cantilever Wall Buildings to Strong Pulse - Type Seismic Excitation

Vladimir Calugaru[‡] and Marios Panagiotou[*,†,§]
Department of Civil and Environmental Engineering, University of California, Berkeley, CA, USA

SUMMARY

This report investigates the seismic response of tall cantilever wall buildings subjected to pulse-type ground excitation, with special focus on the relation between the characteristics of ground motion and the higher-modes of response. Buildings 10, 20, and 40 stories high were designed such that inelastic deformation was concentrated at a single flexural plastic hinge at their base. Using nonlinear response history analysis, the buildings were subjected to near-fault seismic ground motions as well as simple close-form pulses, which represented distinct pulses within the ground motions. Euler-Bernoulli beam models with lumped mass and lumped plasticity were used to model the buildings. The response of the buildings to the close-form pulses fairly matched that of the near-fault records. Subsequently, a parametric study was conducted for the buildings subjected to three types of close-form pulses with a broad range of periods and amplitudes. The results of the parametric study demonstrate the importance of the ratio of the fundamental period of the structure to the period of the pulse to the excitation of higher modes. The study shows that if the modal response spectrum analysis approach is used—considering the first four modes with a uniform yield reduction factor for all modes, and with the square root of sum of squares modal combination rule—it significantly underestimates various response parameters. A response spectrum analysis method that uses different yield reduction factors for the first and the higher modes is presented.

KEY WORDS: higher-modes; near-fault; pulse-type ground motion; structural walls; tall buildings;

INTRODUCTION

The inelastic response of tall reinforced concrete wall buildings is greatly affected by higher-mode effects. This phenomenon was first demonstrated by the pioneering analytical work of Blakeley *et al.* [1] and has been corroborated by various analytical [2–8], small-scale [9] experimental, and large-scale [10, 11] experimental studies. The higher modes significantly affect the acceleration, force, and displacement inelastic seismic response of reinforced concrete wall buildings.

---

[*]Correspondence to: Marios Panagiotou, Department of Civil and Environmental Engineering, University of California, Berkeley, CA, U.S.A.

[†]E-mail: panagiotou@berkeley.edu

[‡] Graduate Student Researcher.

[§]Assistant Professor.

Seismic design of buildings for a code-prescribed design level earthquake recommends using reduced design lateral forces as opposed to the elastic ones, accepting the possibility of nonlinear deformations occurring in parts of the structural system. Current design procedures include methods consistent with traditional capacity design concepts [12], where parts of a structure are intended to remain elastic, and nonlinear deformations are restricted to regions defined as plastic hinges. Building codes [13] include prescriptive requirements to ensure the withstanding of deformation demands in plastic hinge regions. In reinforced concrete (RC) wall buildings, a single plastic hinge is selected to develop at the base of walls in vertically regular buildings [4, 10, 13–18]. Capacity design of wall regions other than the plastic hinges, assuming an essentially elastic response, requires estimating the bending moment and shear force demands.

To ensure elastic response in regions other than the plastic hinges, several seismic design codes [15–17] account for higher-mode effects by proposing a design bending moment envelope that varies linearly from the expected flexural overstrength at the wall base to zero at the top. Studies have found that such a linear envelope does not always preclude the spread of plasticity into regions above the bottom plastic hinge [7, 18–21]. For the shear design envelope, the NZS 3101 code [16] uses an empirical factor that accounts for flexural overstrength and higher-mode response by amplifying the first mode design shear forces. The EC8 [15] proposes that design shear forces be taken at least 50% larger than the shear forces obtained from analysis, with the design shear force at any point along the height of the building to be taken as larger than 50% of the amplified base shear force. According to EC8, the magnification factor of shear forces can be as large as the behavior factor, q, used in the design.

The design force envelopes in tall RC wall buildings are commonly estimated by modal response spectrum analysis (MRSA), using an accepted modal combination method such as the square root of sum of squares (SRSS). Elastic forces obtained from the modal combination are reduced by a response modification factor, R, to obtain the design forces. Performing MRSA using SRSS and an R, uniform to all the modes, will be termed MRSA throughout this paper.

Research on RC cantilever wall buildings has shown that flexural yielding at the base reduces mainly the first-mode response [3, 10, 11, 19-22]; therefore, the relative contribution of the higher modes to response quantities increases with increasing ground motion intensity. Using MRSA, results in non-conservative estimates of seismic demand in nonlinear cantilever walls. For frame structures it has been also shown that nonlinear response reduces more the first than the higher modes of response [23, 24].

A simplified modal superposition method proposed by Eibl [3] considers only the first two modes of response, with a response modification factor applied only at the first mode, i.e., the second mode of response is considered elastic. For the case of near-fault ground motions, Panagiotou and Restrepo [11] proposed a method that considers only the first two modes of response with different response modification factors in each of them. Researchers demonstrated that applying MRSA using the SRSS combination method—where the higher modes are considered to be elastic—provide a satisfactory estimate of acceleration [22] and force [19, 21] response parameters. Chopra and Goel [24] proposed a similar approach for frames, which was evaluated in terms of story drifts, not forces.

Although previous research has investigated the effects of near-fault ground motions on the inelastic response of steel frame [25–31], RC frame [32, 33], and wall [11, 20, 34] buildings, none of these studies focusing on RC walls have investigated this effect for a broad range of pulse waveform, period, and amplitude. This type of ground motions can cause significant inelastic deformation demands with concurrent strong excitation of the higher than the first

modes of response. Nor have these studies investigated this effect on a broad range of inelastic response quantities, i.e. section curvatures, floor accelerations, story shear forces, and story bending moments.

This study investigates the inelastic response of tall reinforced concrete cantilever wall buildings subjected to strong pulse-type ground motion. Emphasis is given to the relationship between the ground motion characteristics and higher-mode response. The study explores the accuracy of simplified close-form representations of pulse-type near-fault ground motions to compute the inelastic response. The response parameters considered are base section curvature, floor accelerations, bending moments, and shear forces. Three types of close-form pulses with a broad range of periods and amplitudes are considered. In order to evaluate the efficiency of MRSA, this study compared the response obtained using MRSA and nonlinear dynamic response history analysis (NDRHA). This study then went on to develop a modified modal response spectrum analysis (MMRSA) approach that considers only the first three modes of response using different yield reduction factors in the first and higher-modes.

NEAR-FAULT GROUND MOTIONS AND THEIR CLOSED-FORM REPRESENTATION

Near-fault ground motion records may contain high amplitude acceleration, velocity, and displacement pulses [35]. High amplitude low frequency pulses are contained in far field ground motions affected mostly by site effects. The waveform, number of cycles, predominant period, and amplitude of the pulses determine the motion's damage potential for different structures [20, 25-34, 36–42]. For near fault ground motions these pulse characteristics depend roughly on the fault type and orientation, as well as the direction of rupture propagation [35].

Several approaches use close-form mathematical pulses or waveforms [37–44] that approximate the distinct pulses observed in the displacement, velocity, and acceleration time histories of strong near-fault ground motions. Such approximations capture many of the characteristics of the corresponding ground motions and allow for parametric numerical studies of structures where the relationship between the structural period and the pulse period can be explored.

This study reported herein uses the close-form representation of near-fault ground motions as described by Makris [38]. Figure 1(a) shows the displacement, velocity, and acceleration histories of three close-form pulses. Pulses A and B are described by a one-sine and one-cosine acceleration time history, respectively. Pulses A and B have a duration equal to their period, T_p, while the duration of Pulse C is equal to $1.43T_p$. Figure 1(b) and (c) depict the elastic single degree of freedom (SDOF) oscillator acceleration and displacement response spectra, respectively, of the pulses for viscous damping ratio ζ = 2%. The spectra are presented in terms of T / T_p, where T is the period of the oscillator. Spectral acceleration S_a is normalized by the peak pulse acceleration amplitude, a_p, while the spectral relative displacement S_d is normalized by $a_p \cdot T_p^2$.

Figure 2(a) depicts the ground acceleration time histories of three strong near-fault ground motions. The RRS228 and JFA292 records are from the Mw 6.7 1994 Northridge earthquake, and the PCD164 record is from the Mw 6.6 1971 San Fernando earthquake. Figure 2(b) shows the velocity time histories of the ground motions, and Figure 2(c) plots the absolute acceleration response spectra for ζ = 2%. Pulses A, B, and C approximate distinct pulses observed in the time histories of the RRS228, JFA292, and PCD164 records, respectively. The pulse parameters were

selected to provide a fit of the strong pulses recorded in the velocity time histories. The velocity pulse amplitudes, v_p, used to represent the RRS228, JFA292, and PCD164 records are 1.66, 0.73, and 0.82 m/sec, respectively, while the corresponding values of T_p are equal to 0.78, 0.99, and 1.24 sec. For the JFA292 record, pulse B was used to approximate only the first of the two distinct pulses contained in the velocity record.

Figure 2(c) depicts the elastic acceleration response spectra of the close-form pulses. For the RRS228 record, the pulse approximation resulted in a fair estimation of the spectral acceleration. Underestimation of the spectral acceleration is observed for T smaller than 1.6 sec. For the JFA292 record, the pulse approximation did not adequately estimate spectral accelerations, especially in the period range between T = 1 to 2.5 sec. This is due to the lack of representation of the second distinct pulse observed in the velocity and acceleration time histories of the JFA292 record. For the PCD164 record, the close-form pulse estimated spectral accelerations with high accuracy for cases where T was longer than 0.8 sec and shorter than 4.0 sec. Pulse C in this case could not estimate spectral accelerations when T was less than 0.8 sec. This is because the spectral acceleration in this period range was due to the strong high-frequency spikes observed in the time, t, history after t = 4 sec.

Figure 3 compares the response spectra for the considered RRS228, JFA292 and PCD164 recorded ground motions to the design base earthquake (DBE) and maximum considered earthquake (MCE) spectra, based on ASCE-7 [14], for the corresponding station locations, where the motions were recorded. For all the three ground motions considered the spectral accelerations around the predominant period, T_p, as defined above, significantly exceed the spectral accelerations of the MCE spectra. For the JFA292 this is true in the period range of the second distinct velocity pulse with T_p of about 1.58 sec that exists in this record and is not approximated in this study. The spectral accelerations at T_p are 1.76, 1.63, and 1.60 times the MCE spectral acceleration for the RRS228, JFA292 and PCD164 records, respectively.

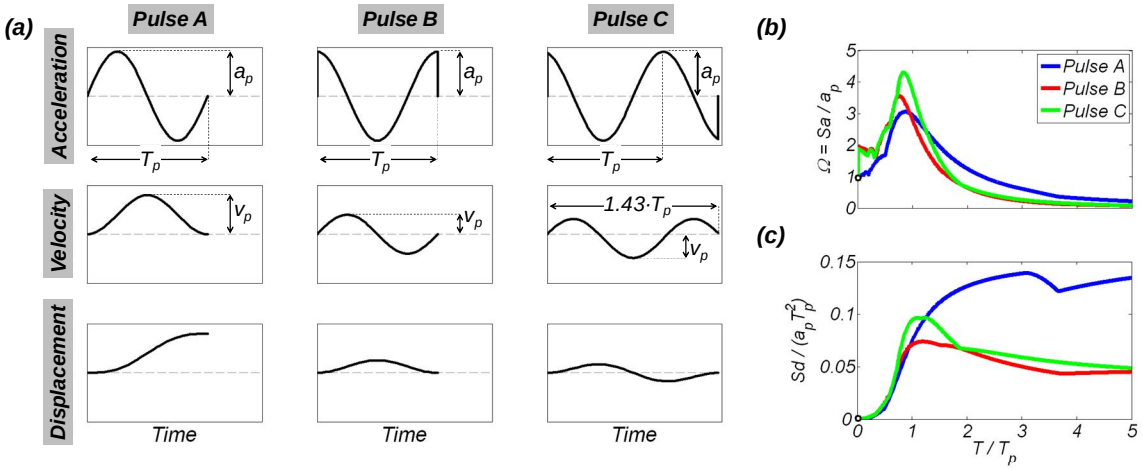

Figure 1. (a) Acceleration, velocity, and displacement time histories; (b) absolute acceleration; and (c) relative displacement response spectra of the three close-form pulses considered, ζ = 2%.

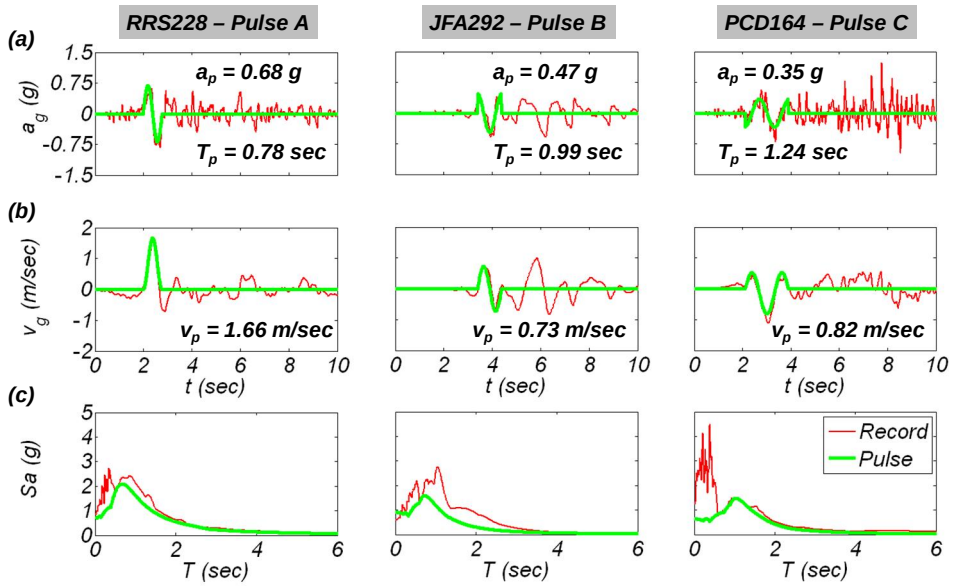

Figure 2. (a) Acceleration; (b) velocity time histories of ground motions considered and their close-form pulse approximation; and (c) elastic SDOF absolute acceleration response spectra of ground motions and their close-form pulse representation, $\zeta = 2\%$.

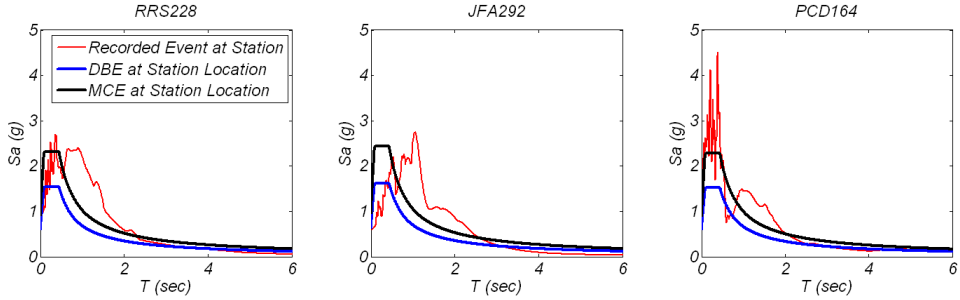

Figure 3. Response spectra for the considered ground motions compared to DBE and MCE spectra, based on ASCE-7, at the station locations of the records.

NUMERICAL ANALYSES RESULTS

The results of numerical analyses of the 10-, 20-, and 40-story buildings are presented next. First, modal analysis of the buildings is performed and then, NDRHA of the buildings subjected to the near-fault ground motions and to their pulse approximations, described above, is conducted. Finally, the results of the parametric NDRHA study of the buildings subjected to the three close-form pulses of various amplitudes a_p and periods T_p are presented, and the efficiency of MRSA is evaluated.

Buildings description and modeling

Reinforced concrete core-walls provide all the lateral force resistance for these buildings. Figure 4 shows the floor, core wall, and gravity column dimensions and layout for the three buildings. Table 1 lists the main characteristics of these buildings, including the floor height *h*, the building height *H*, the seismic weight per floor *w*, the axial load per floor ΔP_W and ΔP_C acting on the wall and the gravity columns, respectively, as well as the main characteristics of the core-wall and gravity columns. P_{bw} and P_{bc} are the axial loads at the base of the core walls and gravity columns with the highest axial load, respectively. The nominal compressive strength of concrete is $f_c^{'}$ = 41.4 MPa for the 10-story building, and $f_c^{'}$ = 55.2 MPa for the 20- and 40-story buildings.

The buildings are designed to allow the formation of a single flexural plastic hinge extending over the bottom 10% of the building height (see Figure 5(a)). The design of the buildings based on ASCE-7 [14] is discussed in the section *Design of Buildings*. The reinforcing steel ratio in the plastic hinge region $\rho_{l,b}$ is equal to 1.27%, 1.32%, and 0.81% for the 10-, 20-, and 40-story buildings, respectively. The remaining portion of the wall is considered essentially elastic, assuming adequate amount of longitudinal reinforcement is provided. Expected flexural strengths, $M_{b,y}$, and the corresponding yield curvatures, φ_y, were calculated by moment-curvature analysis using the provided reinforcement and axial loads, see Table 1. The total seismic weight of the building is W_t.

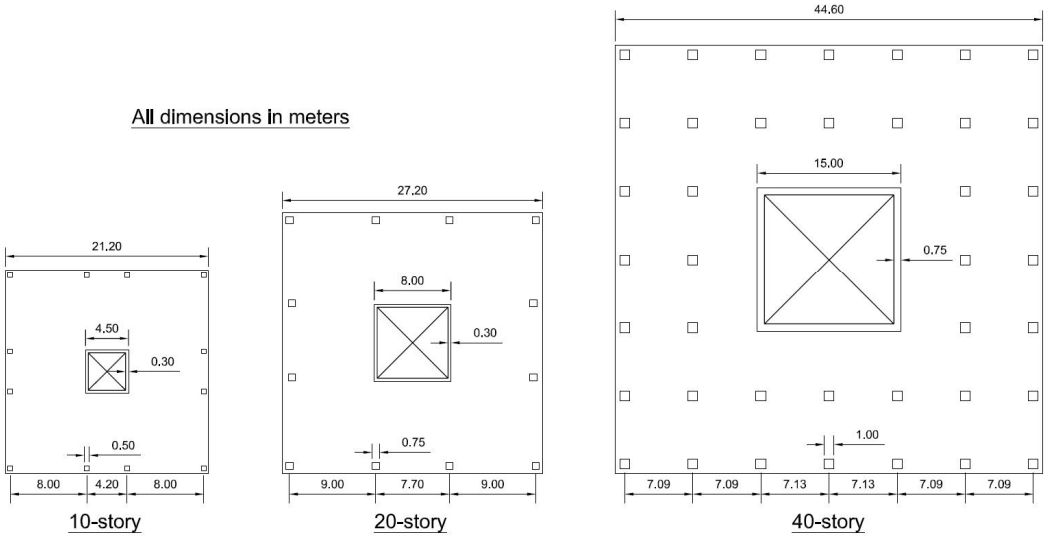

Figure 4. Floor plan-view of the 10-, 20-, and 40-story buildings.

All floors had identical lumped mass, *m*, see Figure 5(b). One-component Giberson beam elements [45] were used to model the walls. One such beam element represents a core-wall segment between two consecutive floors. The plastic hinge length at each end was assumed to be half the element length. The moment-curvature hysteretic response in the plastic hinges was represented by the Clough [45] hysteretic rule, see Figure 5(c). Using expected yield flexural strength M_y and the yield curvature φ_y, the effective flexural rigidity of the beam element was given by $EI_e = M_y / \varphi_y$. A post-yield flexural rigidity ratio *r* equal to 0.02 was computed from moment-curvature analysis. The elastic portions of the walls were modeled with elastic elements, with $EI_e = 0.4EI_g$, where I_g is the gross-section moment of inertia and *E* the initial concrete

modulus. The effect of EI_e value was investigated below, considering also the cases of EI_e equal to $0.2EI_g$ and $0.6EI_g$. In this model, the flexural rigidity ignored completely the tension stiffening effect. Tension stiffening affects the initial period of the buildings and can also affect the response, especially in cases of limited nonlinear response or lightly reinforced walls. The stiffness and strength of the gravity load system was not considered, and all walls were fixed at their base. The cumulative flexural strength of the gravity columns at their base was calculated to be less than 9% of the corresponding strength of the core walls for all three buildings, see Table 1. The longitudinal steel ratio of the gravity columns was ρ_{gc} = 1.5%. This study ignored the effect of shear deformations. The lumped-plasticity model used did not consider the effect of axial force–bending moment–shear force interaction in the nonlinear hysteretic behavior of the walls. The computer program Ruaumoko [45] was used to perform the NDRHA, and large displacement theory was selected for the analyses. Caughey constant 2% viscous damping ratio was used in all the modes [45, 46]. The effect of the damping model is investigated in the *Effect of Damping Model* section.

Table 1. Building characteristics.

Building	10-story	20-story	40-story
Floor height, h (m)	3.35	3.35	3.35
Building height, H (m)	33.5	67.1	134
Seismic weight / floor, w (kN)	4827	6829	19195
Axial load / floor in core wall, ΔP_W (kN)	1813	2754	8135
Axial load / floor in gravity columns, ΔP_C (kN)	3014	4075	11060
Length of core wall, L_w (m)	4.5	8	15
Core wall thickness, t_w (m)	0.3	0.3	0.75
Core wall base axial load ratio $P_{bw} / (f_c^{'} A_{gw})$	0.09	0.11	0.14
Longitudinal reinforcement steel ratio at core wall's base, $\rho_{l,b}$ (%)	1.27	1.32	0.81
Base expected yield flexural strength of core wall, $M_{b,y}$ (kN·m)	94582	405030	3305770
Base expected yield curvature of core wall, φ_y (Rad/m)	7.49E-4	4.50E-4	2.36E-4
EI_e / EI_g for plastic hinge region of core wall	0.31	0.36	0.35
Design Shear Stress of Core Walls based on $1.25M_{b,y}$ (MPa)	1.59	2.31	2.33
Curvature Ductility at 5% tensile strain of steel, $\mu_{\varphi,5\%}$	16.3	14.8	15.2
Side dimension of square gravity columns (m)	0.50	0.75	1.0
Gravity columns base axial load ratio, $P_{bc} / (f_c^{'} A_{gc})$	0.24	0.22	0.20
Sum of expected flexural strength of gravity columns / $M_{b,y}$	0.086	0.082	0.078
Normalized design base moment, $M_u / W_t H$	0.042	0.027	0.0237
Normalized design base shear corresponding to M_u, V_u / W_t	0.088	0.074	0.074

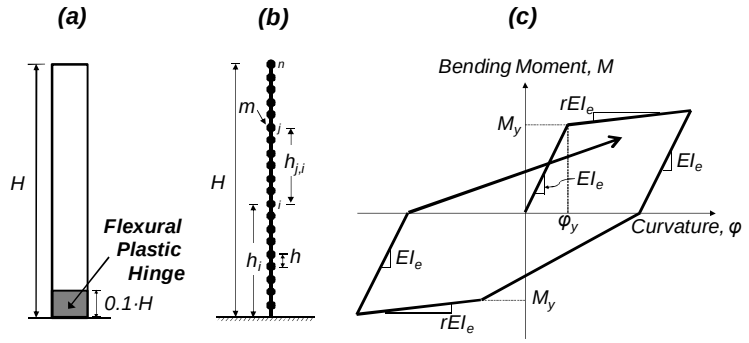

Figure 5. (a) Flexural plastic hinge definition; (b) mass distribution of the lumped-mass Euler-Bernoulli cantilevers; and (c) idealized moment-curvature hysteretic response.

Design of Buildings

The buildings were designed according to the ASCE 7 [14] seismic design requirements for a site in downtown Pasadena, CA, for soil type C, corresponding to very dense soil and soft rock. Figure 6 depicts the DBE and MCE acceleration and displacement spectra for the site considered. For the specific site S_S = 2.53 g, S_1 = 0.87 g, S_{DS} = 1.68 g, and S_{D1} = 0.75.

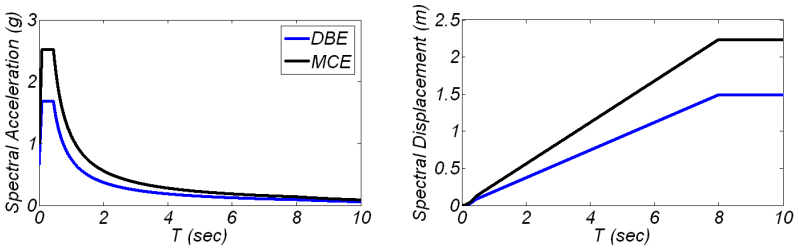

Figure 6. Acceleration and displacement design spectra for a site in downtown Pasadena, CA.

Modal response spectrum analysis (MRSA), based on the requirements of ASCE-7, with a response modification factor of R = 5 was used to obtain design forces. The design bending moment, M_u, and shear force, V_u, envelopes are shown in Figure 7 and are also reported in Table 1. An effective section moment of inertia $I_e = 0.5I_g$ was used for the core-walls along their entire height elements for the MRSA. In Figure 7, the MRSA bending moment and shear force envelopes for this design model are labeled *MRSA*. Based on section 12.9.4 of ASCE-7 the design base shear force can't be less than 85% of the base shear force, $V_{b,ELFP}$, required based on the equivalent lateral force procedure (ELFP). This requirement controlled the design shear forces for the 20-, and 40-story buildings. The envelopes, termed $MRSA_{VELFP}$ in Figure 7, are the MRSA envelopes scaled up by $0.85\frac{V_{b,ELFP}}{V_{b,MRSA}}$, where $V_{b,MRSA}$ is the base shear force computed with MRSA. The $MRSA_{Mb,o}$ envelopes, shown also in Figure 7, are the *MRSA* envelopes scaled by $1.25\frac{M_{b,y}}{M_{b,MRSA}}$, where 1.25 is the base flexural overstrength factor, and $M_{b,MRSA}$ is the *MRSA* base bending moment.

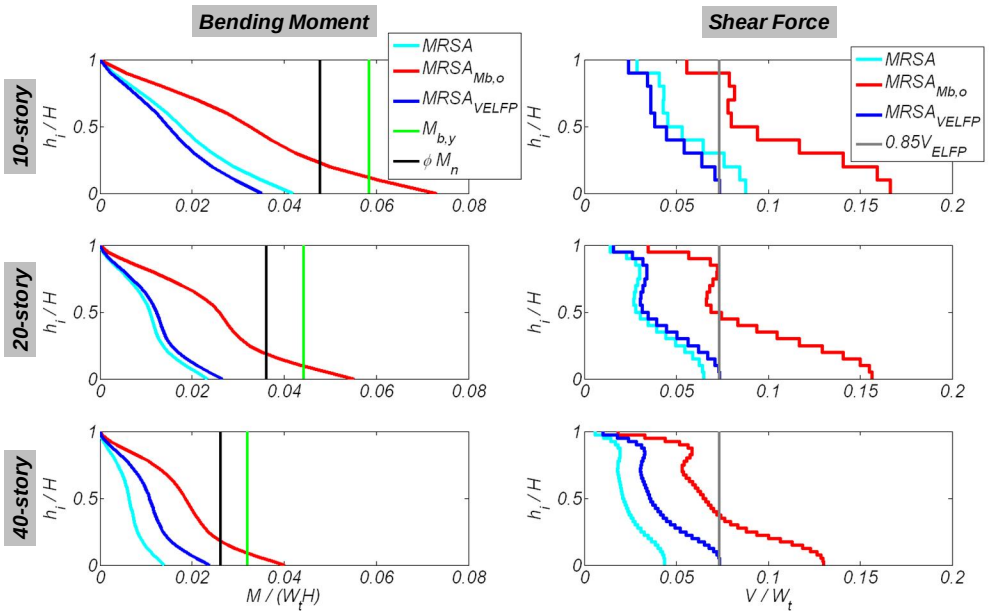

Figure 7. Design bending moment and shear force envelopes based on MRSA.

Modal analysis

Figure 8 and Table 2 present the main modal characteristics of the first three modes of the buildings considered. The buildings termed 10-, 20-, and 40-story are these with $EI_e = 0.4EI_g$ for the elastic parts of the walls. Figure 8 also includes the modal characteristics of the 20-story building using the reduced flexural rigidity (RFR), rEI_e, defined in Figure 5(c), for the plastic hinge elements. The modal characteristics of the 20-story building with $EI_e = 0.2\ EI_g$ used for the elastic portions of the wall, termed 20-story-$0.2EI_g$, are also presented in Figure 8.

The normalized modal characteristics presented are: (a) modal lateral force; (b) modal bending moment; and (c) modal shear force diagrams for the first three modes. The normalized modal lateral force of mode q at floor i, $r_{F,q,i} = F_{q,i} / (m \cdot A_q)$, is equal to the ratio of lateral force due to mode q, $F_{q,i}$, to the product of the modal acceleration, A_q, and the floor seismic mass, m [46]. Equation 1 relates $F_{q,i}$ to the product of $\Gamma_q \Phi_{q,i}$, where Γ_q is the modal participation factor and $\Phi_{q,i}$ is the value of the modal vector of mode q at floor i. The normalized modal shear force, $r_{V,q,i} = V_{q,i} / (m_t \cdot A_q)$, is equal to the ratio of the shear force at floor i due to mode q, $V_{q,i}$, to the product of the total seismic mass, m_t, times A_q. $V_{q,i}$ is calculated using Equation 2. The normalized modal base shear force is equal to the effective modal mass m_q [46] normalized by m_t. The normalized modal bending moment, $r_{M,q,i} = M_{q,i} / (m_t \cdot H \cdot A_q)$, is equal to the ratio of the bending moment at floor i due to mode q, $M_{q,i}$, to m_t times the height, H, of the building times A_q. $M_{q,i}$ is calculated using Equation 3. The term $h_{j,i}$ is defined in Figure 5(b).

$$F_{q,i} = \Gamma_q \cdot \Phi_{q,i} \cdot m \cdot A_q \tag{1}$$

$$V_{q,i} = \sum_{j=i}^{n} \Gamma_q \cdot \Phi_{q,j} \cdot m \cdot A_q \tag{2}$$

$$M_{q,i} = \sum_{j=i}^{n} \Gamma_q \cdot \Phi_{q,j} \cdot m \cdot h_{j,i} \cdot A_q \tag{3}$$

The normalized modal characteristics of the 10-, 20- and 40- story buildings, with EI_e = 0.4 EI_g for the walls' regions above the base plastic hinge, were practically identical, indicating insensitivity to the number of floors. For these three buildings, the peak normalized first and second mode bending moment occurred at their base. The absolute value of the second mode bending moment at mid-height was close to the corresponding value at the base of the wall. The values of the normalized third mode bending moment along the building heights were small. Same sign of first and second mode accelerations resulted in modal bending moments and shear forces at the base of same sign, while they resulted in mid-height modal bending moments of different sign. Reduction of flexural rigidity at the base (see Figure 8 for the 20-story-RFR building) resulted in a straighter first-mode lateral force diagram without any significant change in its value at the top of the building, resulting in an increase of the normalized effective first modal mass.

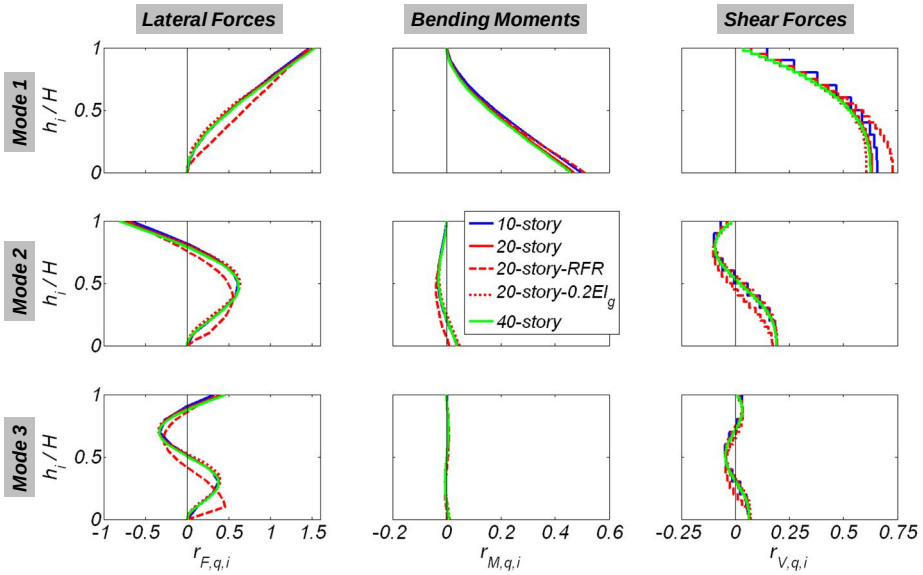

Figure 8. Normalized modal characteristics of the buildings.

Table 2 summarizes the main modal characteristics of four of the buildings considered. For the buildings with EI_e = 0.4EI_g, the ratios T_1 / T_2 and T_1 / T_3 of the first modal period T_1 to the second and third mode, respectively, were essentially insensitive to the number of stories. The absolute values of the normalized second mode base bending moment were less than one tenth of the corresponding first-mode values for all buildings studied. Thus, inelastic response at the base of the walls should be expected to reduce the first mode of response more than the second. The reduction of flexural rigidity at the base affected mainly the first modal period, elongating it 8.8 times, while the second-mode period was elongated only 1.5 times. The cumulative normalized effective modal mass of the first three modes increased from 0.89 for the 20-story building to 0.97 for the 20-story-RFR building. The 20-story-RFR building had a nearly zero normalized second-mode base bending moment. In this case, base inelasticity is expected to have a limited

effect in reducing the second mode of response. Changing EI_e / EI_g from 0.2 to 0.4 caused only minor changes of the normalized modal characteristics.

We investigated the effect of the gravity system on the stiffness of the buildings. The columns, and the slabs were modeled using Euler-Bernoulli beam elements with effective flexural rigidities at yield, EI_e, based on moment-curvature analysis. The full width of the slabs and the framing between the core walls, the slabs, and the gravity columns were considered. This reduced the first mode period by less than 9% for all three buildings. The corresponding reduction of the second mode period was less than 2%.

Table 2. Main modal characteristics of the buildings.

Mode	Building	10-story	20-story	20-story-RFR	40-story
1	Modal period T_q (sec)	2.2	4.0	35	6.6
2		0.3	0.6	0.9	1.0
3		0.1	0.2	0.3	0.4
2	Modal period ratio T_1 / T_q	6.5	6.4	41	6.5
3		18	18	110	18
1	Normalized modal base shear force (equal to normalized effective modal mass) $r_{V,q,b} = m_q$ / m_t	0.66	0.63	0.73	0.63
2		0.19	0.20	0.17	0.19
3		0.07	0.06	0.07	0.06
1	Normalized modal base moment $r_{M,q,b}=M_{q,b}$ / (m_t·H·A_q)	0.497	0.470	0.511	0.459
2		0.039	0.040	0.010	0.039
3		0.008	0.008	0.003	0.008
1	Normalized modal mid-height moment $r_{M,q,0.5H} = M_{q,0.5H}$ / (m_t·H·A_q)	0.181	0.166	0.170	0.159
2		-0.032	-0.030	-0.038	-0.029
3		-5.8E-4	-2.7E-4	0.005	1.8E-5

Building response to near-fault ground motions and their pulse approximations

Figure 9 presents the NDRHA results for the three buildings, each subjected to one of the near-fault ground motions and its pulse approximation as described above. The base bending moment, M_b, mid-height bending moment, $M_{0.5H}$, base shear force, V_b, and roof absolute acceleration, A_r, response histories are presented. The response quantities are normalized by the maximum of the peak values computed using the near-fault record and its pulse representation. The 10-, 20-, and 40-story buildings were subjected to the JFA292, RRS228, and PCD164 records, respectively. The base curvature ductility, μ_φ, calculated as the peak curvature in the first-story inelastic beam element divided by the yield curvature, φ_y, for the 10-, 20-, and 40-story buildings computed equal to 8.1, 14.1, and 11.6, respectively, indicated highly nonlinear response. Table 1 lists the curvature ductility $\mu_{\varphi,5\%}$ at a tensile strain ε_s = 5% of the extreme section fiber at the base of the wall sections. For all case studies for the duration of the pulse approximation, the computed response using the pulse approximation satisfactorily matched those computed using the near-fault ground motions, except in the case of the base shear force for the 10-story building. For the 20-story building subjected to the RRS228 record, Pulse A provided a satisfactory estimation of peak response quantities. For the 10-story building subjected to the JFA292 record, Pulse B computed satisfactorily the bending moment and roof acceleration response quantities up to the end of the close-form pulse. For the 40-story building

subjected to the PCD164 record, Pulse C computed quite well the different response quantities, even after the end of the close-form pulse and up to t = 6 sec. After t = 6 sec, the response to the near-fault record was dominated by the strong high-frequency excitation, which is not represented by the close-form pulse.

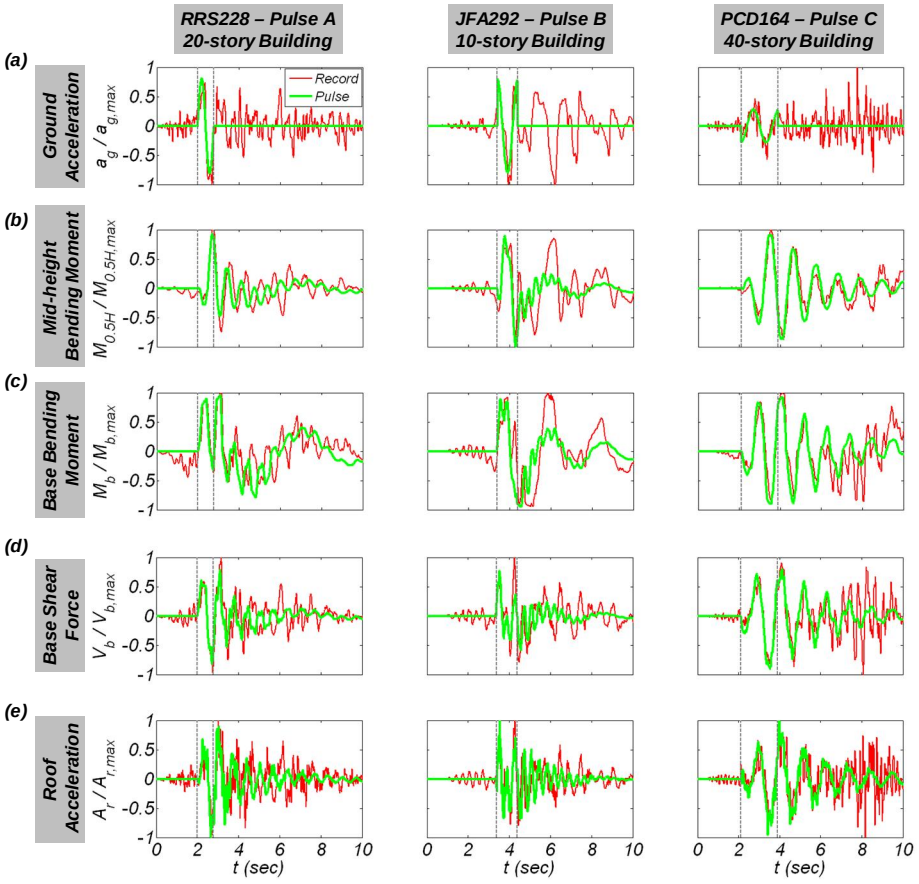

Figure 9. Comparison of the NDRHA results using near-fault ground motions and their close-form pulse approximations. Time histories of (a) ground acceleration, (b) mid-height bending moment, (c) base bending moment, (d) base shear force, and (e) roof absolute acceleration.

For the 20- and 40-story buildings considered, the close-form pulse period was closer to the second modal period of the buildings than to the first-mode period. The T_1 / T_p ratios for the 10-, 20-, and 40- story building case studies are 2.3, 5.1, and 5.3, respectively. The corresponding T_2 / T_p ratios are 0.4, 0.8, and 0.8. Since the pulse period is close to the second modal period of the buildings, significant contribution of the second mode of response is expected, especially for the 20- and 40-story buildings, as shown in Figure 10 for the bending moment, shear force, and acceleration response envelopes computed with NDRHA. The significant effect of the higher modes, especially the second mode, can be seen in all the response quantities for all motions. The peak bending moment around mid-height approached or even exceeded the peak base bending moment for all buildings. The effect of the second mode of response is seen in the shear force envelopes as well, where a local peak was observed close to 80% of the height. This local peak characterizes the normalized second mode shear force diagram, as shown in Figure 8.

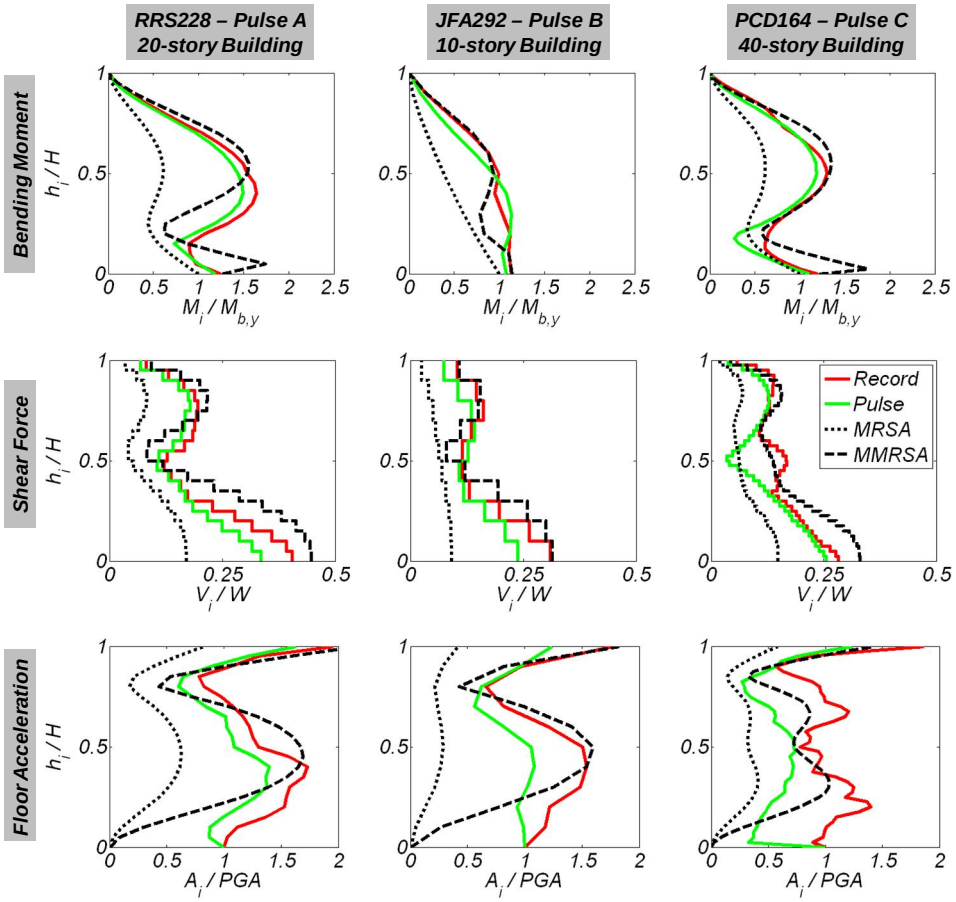

Figure 10. Response envelopes of NDRHA, MRSA, and MMRSA using the near-fault ground motions, and of NDRHA using close-form pulse representations.

The response envelopes computed using the close-form pulses are comparable to those computed with the near-fault records, indicating that the distinct pulses contained in the ground motions determined the response to a large extent. The bending moment and shear force response envelopes computed with the close-form pulses adequately represent those of the near-fault ground motions for the three buildings. Relatively good agreement was also observed in the computed acceleration response for the 20-story building. The largest differences between the responses computed with the near-fault records and their pulse representation is seen in the floor acceleration response, especially for the 40-story building. For this case, floor acceleration response was greatly affected by the higher frequency excitation observed beyond t = 6 sec in the PCD164 record after the end of the approximated pulse (see Figure 9). For this record, a local peak was observed in the shear force envelope around the mid-height of the 40-story building. Here, the high-frequency excitation observed after t = 6 sec significantly excited the third mode of response. Shown in Figure 8, the third mode shear force diagram has a local peak around mid-height. The acceleration spikes of the PCD164 record after t = 6 sec, see Figure 2(a), resulted in significant spectral accelerations at T = 0.4 sec, see Figure 2(c), which was equal to the third modal period of the building. The following section presents a parametric study of the three buildings subjected to the three pulses, for the amplitude and periods of various pulses.

Building response to close-form pulses and comparison of NDRHA and MRSA

Results of the NDRHA of the three buildings subjected to the close-form Pulses A, B, and C are presented below. Pulse periods T_p corresponding to T_1 / T_p ratios 0.25, 0.50, 0.75, and 1.0 through 20.0, with a step of 1.0, are considered to cover a range extending from low- to high-frequency of excitation. To investigate different levels of inelasticity on the response, different amplitudes a_p for each pulse of period T_p were investigated. For each T_p, the amplitude a_p was determined from the MRSA considering the first four modes. Once the modal characteristics of the buildings were determined, the SRSS combination method was used and a uniform reduction factor R was applied to all modes. By setting the moment demand at the base of the wall equal to the yield base moment strength $M_{b,y}$, the required pulse amplitude was calculated as:

$$a_p = \frac{R \cdot M_{b,y}}{m_t \cdot H \cdot \sqrt{\sum_{q=1}^{4} \left[r_{M,q,b} \cdot \Omega_q \right]^2}} \tag{4}$$

where $r_{M,q,b}$ is the normalized base modal bending moment, see Table 2, and $\Omega_q = Sa(T_q) / a_p$, see Figure 1(b), where $Sa(T_q)$ is the q^{th} mode elastic SDOF spectral acceleration. The cumulative normalized effective modal mass of the first four modes considered was more than 0.9 for all buildings.

Figure 11 plots the calculated values of a_p for the three buildings versus T_1 / T_p for Pulses A, B, and C; values of a_p are normalized by R times the acceleration of gravity g. The secondary (top) x-axis shows also the points that correspond to T_2 / T_p and T_3 / T_p ratios equal to one. In general, a_p increased with increasing T_1 / T_p ratio for all three pulses. For the specific buildings considered in this study for a given T_1 / T_p and R, the required a_p decreased with an increase in the building height. For the 20-story building with T_1 = 4.0 sec for T_1 / T_p = 5 and pulse A, a_p / R = 0.28g. In this case, T_p = 0.8 sec and R = 2.4, a_p = 0.68g. This might represent the case of the 20-story building subjected to the pulse approximation of the RRS228 record with a_p = 0.68g and T_p = 0.78 sec (see Figure 2). For the three buildings, high values of T_1 / T_p and R resulted in very large values of a_p, which are not found in existing near-fault records. That said, these cases are still worth considering for exploring the effect of decrease of T_p (increase of T_1 / T_p) and the effect of increase of a_p.

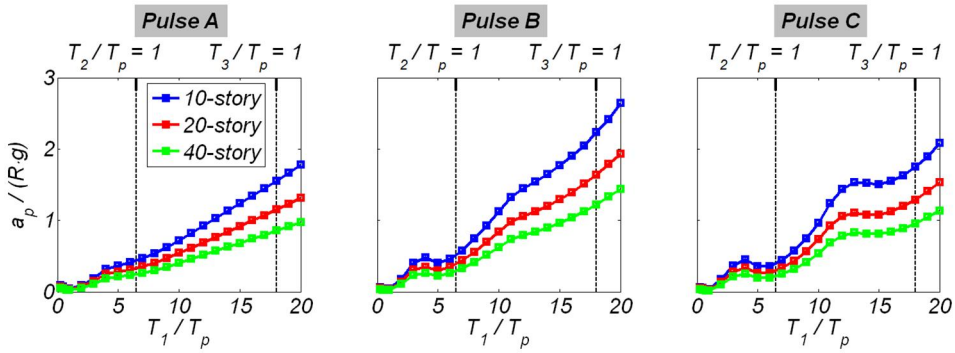

Figure 11. Acceleration amplitude a_p of close-form Pulses A, B, and C versus T_1 / T_p computed with MRSA and a uniform R to all modes, resulting in a base bending moment equal to $M_{b,y}$.

Figures 12 to 14 compare the DBE and MCE design spectra to the spectra of pulses A, B, and C, with a_p computed based on Equation 4, for three values of R and three values of T_p. The design spectra are compared to the pulse excitation spectra for the 10-story building in Figure 12. The corresponding comparisons for the 20-, and 40-story buildings are depicted in Figures 13 and 14, respectively. For the 10-story building, $T_p = T_2$, and $R = 2$, the spectral accelerations are close to the corresponding values of the MCE spectrum in the constant acceleration region. For $T_p = T_2$, and R equal to 4 and 6, the spectral accelerations for the pulse motion far exceed the corresponding values of the MCE spectrum in the constant acceleration region. For $T_p = T_2$, all R values, and T larger than 1.0 sec, the spectral accelerations of the pulse motions are smaller than the corresponding magnitude of the MCE spectra, except for pulse A and $R = 6$. For $T_p = 0.5T_1$, $R = 2$, the pulse spectral accelerations are below the MCE for all pulses and periods, except pulse C around $T = T_p = 1.1$ sec. For $T_p = 0.5T_1$ and $R = 4$ the spectral acceleration for the pulse motions exceed the corresponding MCE values for pulses B and C, and T between 0.7 and 2 sec. The same is true for $T_p = 0.5T_1$ and $R = 6$ for all pulses and T between 0.7 and 2.5 sec. For $T_p = T_1$, R equal to 2 and 4, the spectral accelerations for all pulses are lower than the corresponding MCE values. For $T_p = T_1$, and $R = 6$, the spectral accelerations for all the pulse motions exceed the corresponding MCE values for T around $T_p = 2.2$ sec. Observations similar to those for the 10-story building, can be made for the 20-, and 40-story buildings, with noticeable differences due to the increase of T_1 and T_2 with number of building stories.

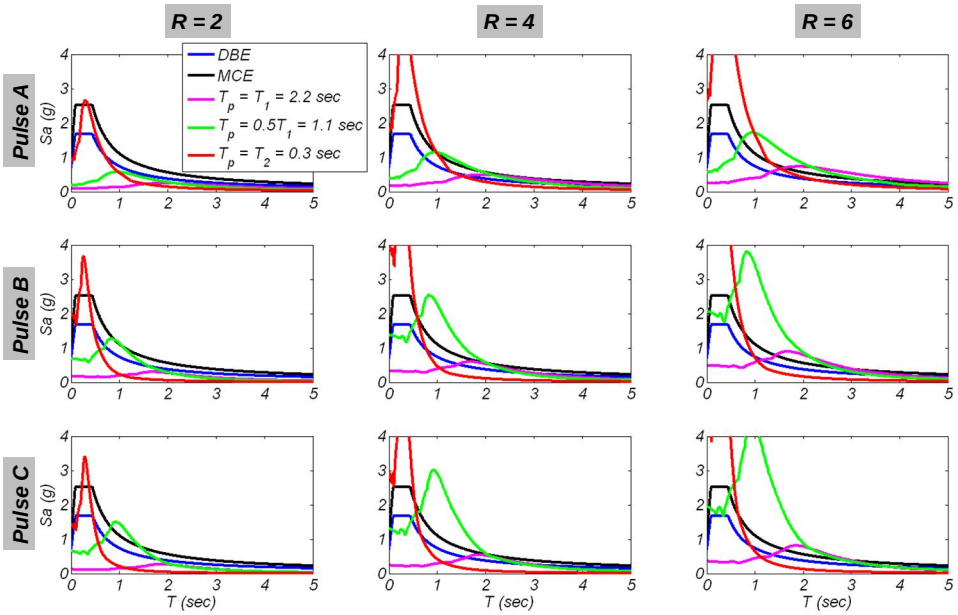

Figure 12. ASCE design basis and maximum considered earthquake and pulse response spectra for the 10-story building.

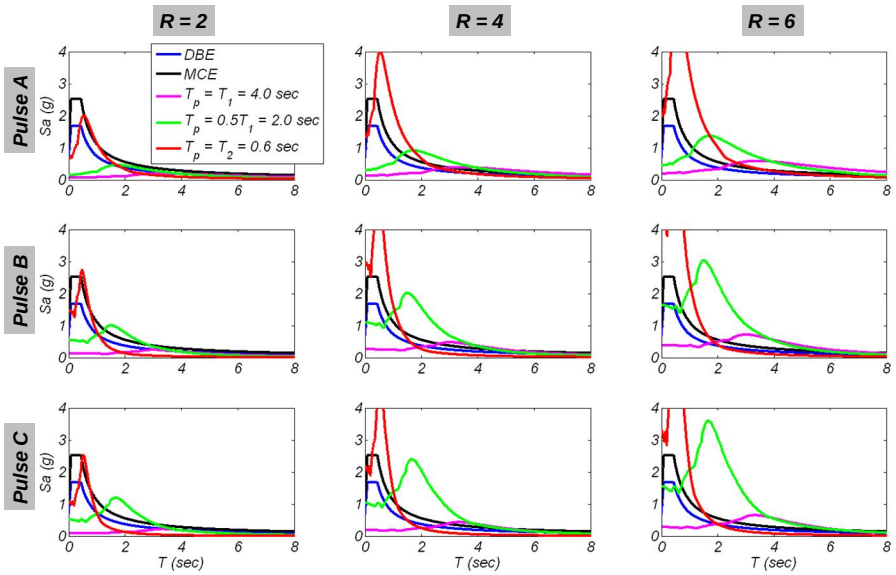

Figure 13. ASCE design basis and maximum considered earthquake and pulse response spectra for the 20-story building.

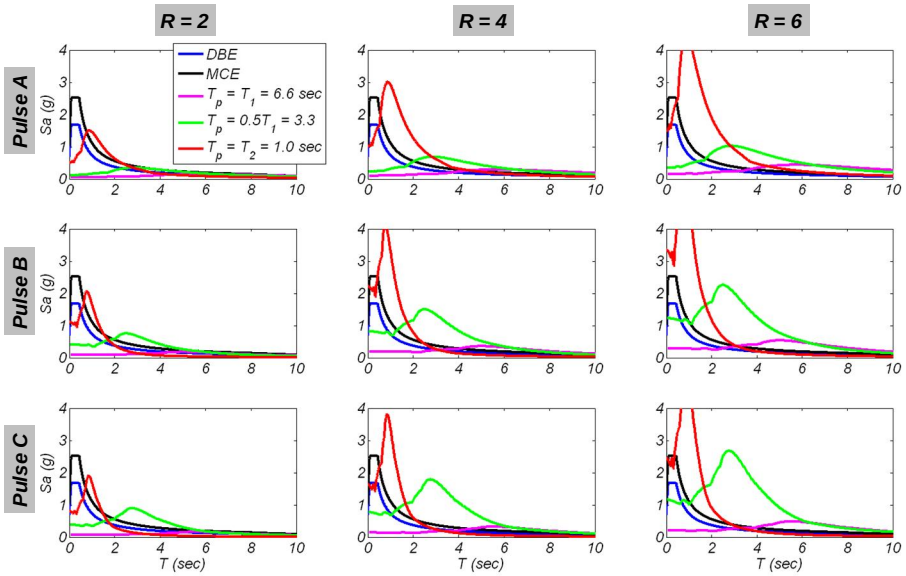

Figure 14. ASCE design basis and maximum considered earthquake and pulse response spectra for the 40-story building.

Figure 15 presents the results of the NDRHA for the three buildings in terms of base curvature ductility $\mu_{\varphi,b}$ calculated as the peak curvature computed at the base of the buildings divided by the yield curvature, φ_y, to Pulses A, B, and C for R = 2, 4, and 6 versus T_1 / T_p. The response parameter $\mu_{\varphi,b}$ indicates the level of inelastic response. As expected for all pulses and buildings, $\mu_{\varphi,b}$ generally increased with increasing R. For T_1 / T_p smaller than 1.0, $\mu_{\varphi,b}$ increased very rapidly with a corresponding decrease of T_1 / T_p. For T_1 / T_p equal to 0.25 or 0.5, the computed values of $\mu_{\varphi,b}$ were virtually unattainable. For T_1 / T_p ratios higher than 1, curvature ductility demands of up to 45 were computed. Excessive and practically unattainable levels of

inelastic response computed for some T / T_p ratios, especially for R = 4 and 6, are worth exploring theoretically. Interestingly, $\mu_{\phi,b}$ attains a local maximum for $T_1 / T_p = 4$, corresponding to $T_2 / T_p = 0.6$, for both $R = 4$ and 6.

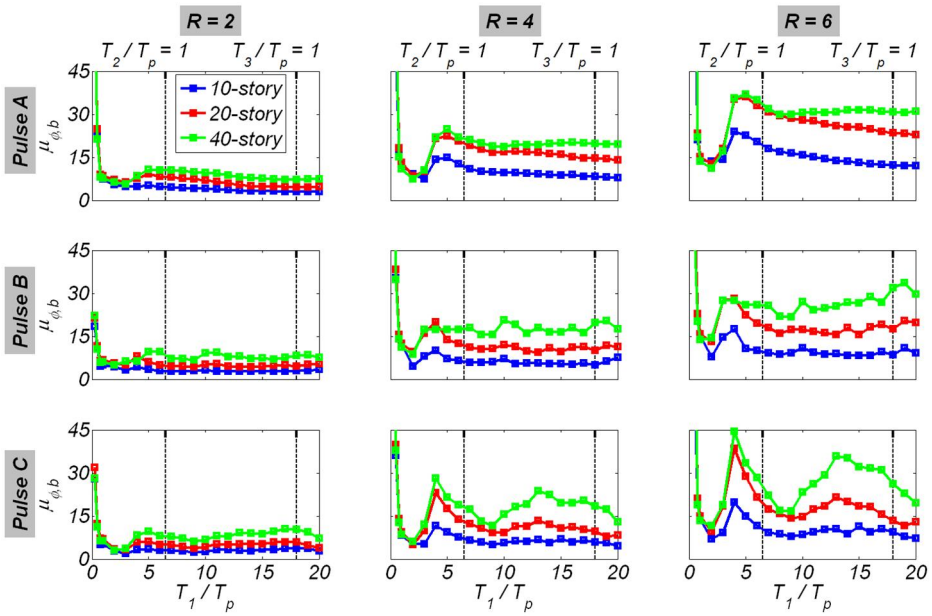

Figure 15. Peak base curvature ductility $\mu_{\phi,b}$ computed with NDRHA.

Figures 16 to 18 present the results of the NDRHA in terms of the mid-height bending moment $M_{0.5H}$, base shear force V_b, and roof absolute acceleration A_r for the three buildings to Pulses A, B, and C, for R = 2, 4, and 6, and for the twenty-three distinct ratios of T_1 / T_p. These response quantities are normalized by those computed by MRSA using a uniform R factor in the four modes.

Figure 16 plots the computed mid-height bending moment in terms of the ratio $\Psi_{M,0.5H} = M_{0.5H,NDRHA} / M_{0.5H,MRSA}$, where $M_{0.5H,NDRHA}$ and $M_{0.5H,MRSA}$ are the peak mid-height bending moments computed by NDRHA and MRSA, respectively. For T_1 / T_p lower than one, corresponding to low-frequency excitation and R equal to 4 and 6, $\Psi_{M,0.5H}$ was much higher than one due to the excessive post-yield section hardening at the base of the walls. Section hardening is not accounted for in MRSA, see Equation 4. For T_1 / T_p higher than one, MRSA significantly underestimated $M_{0.5H}$ for all buildings, all pulses, and all R factors. For all pulses and all R factors, $\Psi_{M,0.5H}$ was more or less independent of the building height and was dependent only on the ratio of T_1 / T_p. For R equal to 4 and 6 and for T_1 / T_p ratios higher than one, maximum values of $\Psi_{M,0.5H}$ occurred at $T_1 / T_p = 4$ for all pulses, except for the 40-story building for Pulse B. For $T_1 / T_p = 4$, corresponding to $T_2 / T_p = 0.6$, significant excitation of the second mode of response occurred. For all the three pulses and for R equal to 4 and 6, $\Psi_{M,0.5H}$ increased rapidly for T_1 / T_p, increasing between 1 and 4. For T_1 / T_p larger than 4, values of $\Psi_{M0.5H}$ were high and of the order of $\frac{2}{3}R$. For $R = 2$, $\Psi_{M,0.5H}$ was nearly uniform and equal to R.

The computed ratio $\Psi_{V,b} = V_{b,NDRHA} / V_{b,MRSA}$, where $V_{b,NDRHA}$ and $V_{b,MRSA}$ are the peak base shear forces computed by NDRHA and MRSA with a uniform R factor in all the modes, respectively, is shown in Figure 17. The variation of $\Psi_{V,b}$ with T_1 / T_p—similar to that of

$\Psi_{M,0.5H}$—was essentially independent of the number of stories, depending mainly on the R factor with a minor sensitivity to the pulse type. For T_1 / T_p lower than one and R equal to 4 and 6, $\Psi_{V,b}$ was much higher than one due to the excessive post-yield base section hardening as explained above. For R equal to 4 and 6, $\Psi_{V,b}$ increased rapidly for T_1 / T_p between 1 and 3 or 4. For R = 4 and 6, and T_1 / T_p larger than one, $\Psi_{V,b}$ attained a maximum value at T_1 / T_p equal to 3 or 4. For R equal to 4 and 6 and for T_1 / T_p larger than 3, $\Psi_{V,b}$ was larger than 0.4R. For R equal to 2, $\Psi_{V,b}$ was nearly constant and equal to R.

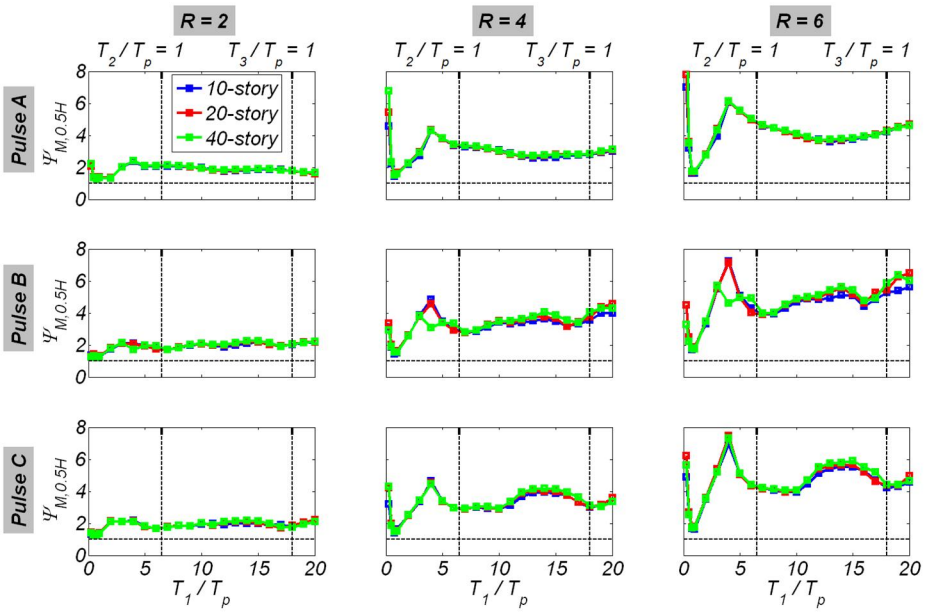

Figure 16. Ratio of peak mid-height bending moments computed with NDRHA and MRSA.

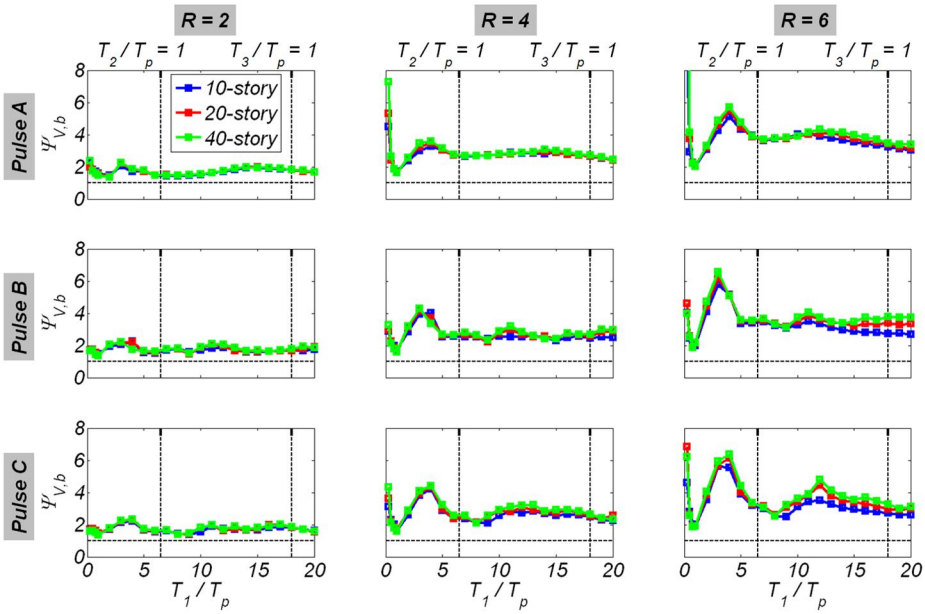

Figure 17. Ratio of peak base shear forces computed with NDRHA and MRSA.

The ratio $\Psi_{A,r} = A_{r,NDRHA} / A_{r,MRSA}$, where $A_{r,NDRHA}$ and $A_{r,MRSA}$ are the peak roof absolute accelerations computed using NDRHA and MRSA with a uniform R factor in all the modes, respectively, is shown in Figure 18. For T_1 / T_p lower than one, $\Psi_{A,r}$ shows similar behavior for the same reasons to that of $\Psi_{M,0.5H}$ and $\Psi_{V,b}$. In general, $\Psi_{A,r}$ increased with R and an increase of T_1 / T_p. For R equal to 2, $\Psi_{A,r}$ was nearly constant and equal to R. Because the normalized NDRHA to the MRSA response was found to be more or less insensitive to the number of stories, only the results for the 20-story building are discussed further.

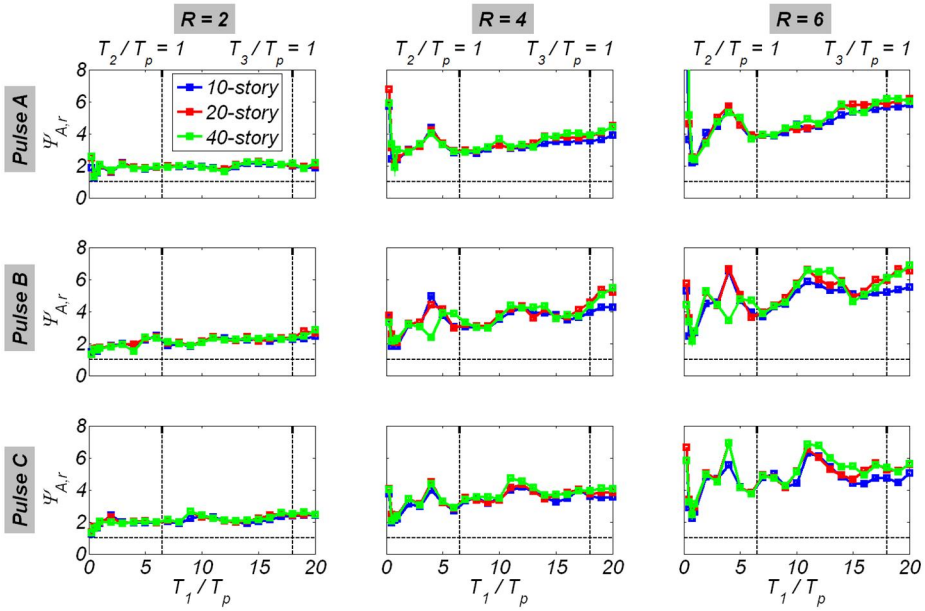

Figure 18. Ratio of peak roof accelerations computed with NDRHA and MRSA.

Figure 19 plots the bending moment envelopes computed by MRSA and NDRHA for R equal to 2 and 6, for four values of T_1 / T_p. The bending moment at floor i, M_i, was normalized by $M_{b,y}$. The envelope computed with MRSA is independent of the value of R since the relative contribution of the modes is independent of R. Values of $M_i / M_{b,y}$ at the base computed with NDRHA were larger than one due to post-yield base section hardening. Compared to NDRHA, MRSA significantly underestimated the bending moment demands in the upper part of the wall. The level of underestimation increased with increasing R.

The amplitude of peak normalized bending moment and the height at which this occurs strongly depends on T / T_p. For values of T_1 / T_p equal to and larger than 3, the bending moment on the upper part of the wall reaches or exceeds the base bending moment yield capacity $M_{b,y}$ in all cases, see Figure 19. For example, for $T_1 / T_p = 6$, Pulse A, and for $R = 2$ and 6, the bending moment at 40% of the height is 1.4 and 3.4 times $M_{b,y}$, respectively, which causes a practical difficulty when trying to ensure elastic response of these regions. If this wall were required to remain elastic, the required longitudinal reinforcement ratio at the eighth story (40% of the height) for Pulse A, $T_1 / T_p = 6$ and $R = 2$ would be 2.8%, an excessively large value. In comparison to the base, the larger bending moment combined with the reduction of axial force resulted in a significant increase in the required longitudinal reinforcement. For $T_1 / T_p = 20$,

corresponding to T_3 / T_p = 1.1, the peak moment based on NDRHA occurred close to 75% of the height, indicating significant contribution of the third mode of response.

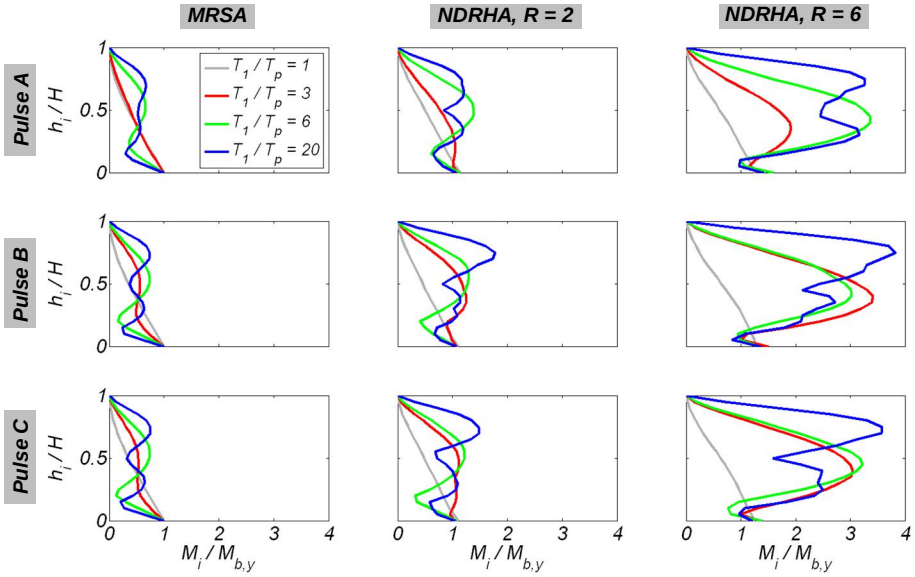

Figure 19. Bending moment envelopes for the 20-story building subjected to pulses A, B, and C for four T_1 / T_p ratios computed with (a) MRSA and NDRHA; (b) R = 2; and (c) R = 6.

Next we investigated the effect of EI_e, used to model the elastic wall regions on the computed ratios $\Psi_{M,0.5H}$, $\Psi_{V,b}$, and $\Psi_{A,r}$ for the 20-story building subjected to Pulse B. Two values of the yield reduction factor, R = 2 and R = 6, and three values of EI_e / EI_g = 0.2, 0.4 and 0.6 were considered. For each value of T_1 / T_p, a_p was recomputed using Equation 4 and accounting for the change in modal characteristics with the corresponding change of EI_e. Figure 20 shows that $\Psi_{M,0.5H}$, $\Psi_{V,b}$, and $\Psi_{A,r}$ are practically independent of the EI_e considered.

The ratio of peak mid-height bending moment $M_{0.5H,max}$ to yield base bending moment $M_{b,y}$ was also investigated (see Figure 21) for EI_e / EI_g equal to 0.2, 0.4, and 0.6, for the 20-story building subjected to Pulse B. For T_1 / T_p lower than one, and R =4 and 6, the ratio $M_{0.5H,max} / M_{b,y}$ was much higher than one because of the excessive post-yield hardening of the base sections. The ratio $M_{0.5H,max} / M_{b,y}$ increased rapidly for values of T_1 / T_p between 1 and 4, reaching a peak at T_1 / T_p between 4 and 8, a period range with significant contribution of the second mode to response. For T_1 / T_p larger than 4, $M_{0.5H,max} / M_{b,y}$ increased with increasing R and increasing EI_e. For $EI_e = 0.4EI_g$, the peak $M_{0.5H,max} / M_{b,y}$ was 1.4, 2.3, and 3.4 for R equal to 2, 4, and 6, respectively.

Finally, the effect of T_1 / T_p on the shear force that developed on the upper part of the buildings was explored. Figure 22 shows the ratio of the peak shear force at three quarters of the wall height, $V_{0.75H,max}$, to the peak base shear force, $V_{b,max}$. Results for the 20-story building for R = 2, 4, and 6 and for all pulses A, B, and C are presented. Small sensitivity of $V_{0.75H,max} / V_{b,max}$ to the pulse type was observed. At T_1 / T_p = 3 corresponding to T_2 / T_p = 0.5 for all R and pulses, the ratio $V_{0.75H,max} / V_{b,max}$ reached its peak value. For all cases except for R = 4 and Pulse A, this peak value was very close or exceeded one. The results presented in Figure 22 indicate that the design shear force at three quarters of the wall height should be at least half of the corresponding value at its base independent of pulse period and R factor.

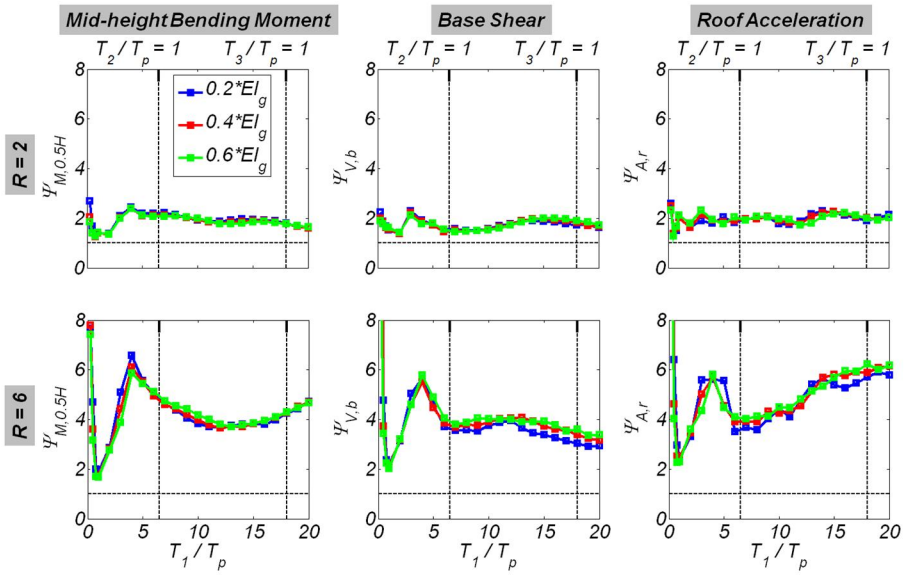

Figure 20. Effect of effective flexural rigidity value on the ratio of responses computed with NDRHA and MRSA for the 20-story building and Pulse B.

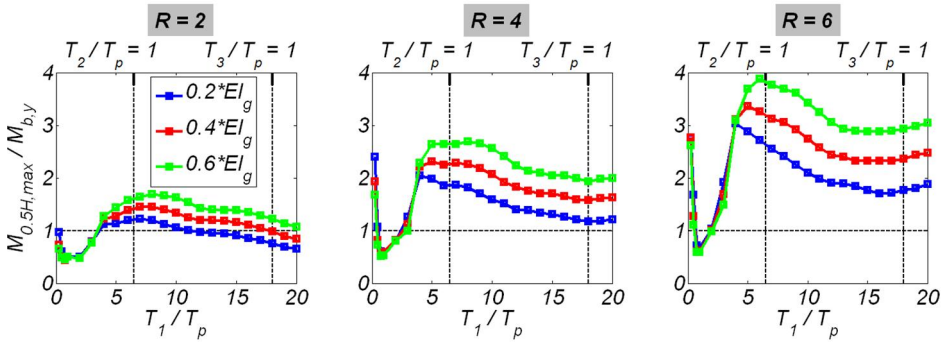

Figure 21. Effect of effective flexural rigidity value, on the ratio of peak mid-height to yield base bending moment computed with NDRHA for the 20-story building subjected to Pulse B.

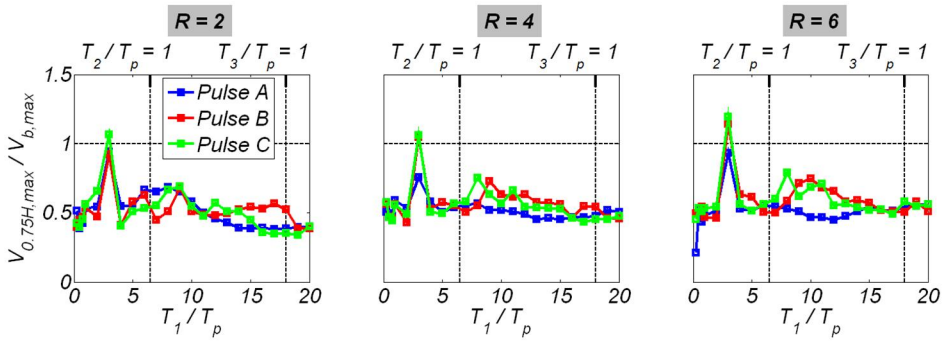

Figure 22. Peak shear force at 75% of the 20-story building's height computed with NDRHA.

Effect of Damping Model

The sensitivity of the building models to the choice of damping model was studied for the 20-story building. Caughey 2% constant damping in modes 1 through 6 was compared to Rayleigh 2% damping in modes 1 and 2, and in modes 1 and 4. Figure 23 and Table 3 show how the Caughey and Rayleigh damping ratio values compare for the first four modes. In comparison with the Caughey damping model the Rayleigh 2% in modes 1 and 2 model results in at least 2.5 times larger damping ratios in modes three and above. In comparison with the Caughey damping model the Rayleigh damping model with 2% damping ratio in modes 1 and 4 results in 3.1 and 1.8 times lower damping ratio in modes 2, and 3, respectively.

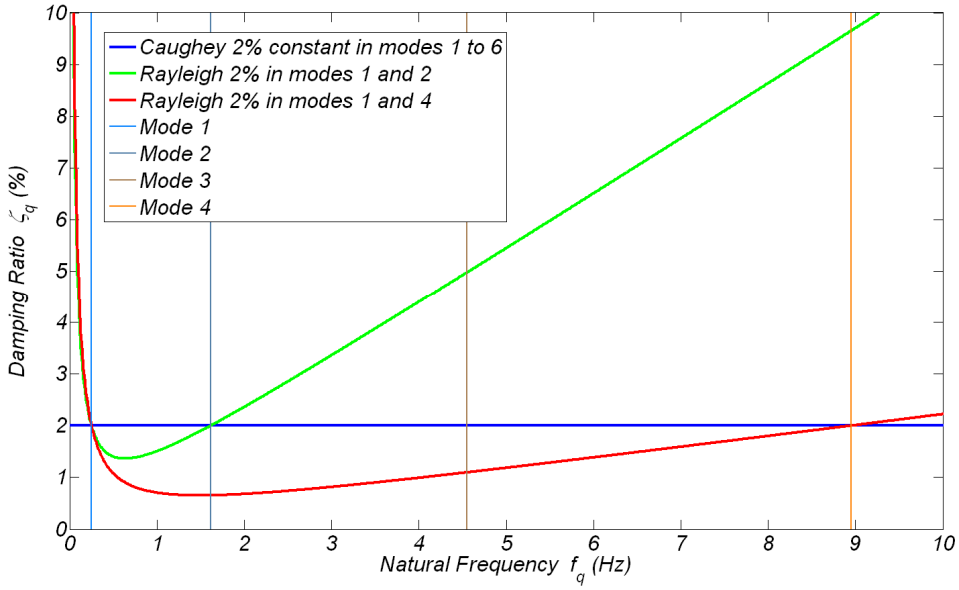

Figure 23. Caughey and Rayleigh damping comparison for the 20-story building.

Figure 24 compares the computed response in terms of four different response parameters (V_b, A_r, $M_{0.5H}$, and $\mu_{\varphi,b}$) for the three damping models for pulse B and R = 4. The larger damping ratios of the Rayleigh damping model with 2% damping ratio in modes 1 and 2, in comparison with the other two models, result in reduction of the different response quantities and especially base curvature ductility, base shear force, and roof acceleration. The effect of the damping model is less pronounced for the mid-height bending moment. The Rayleigh damping model with 2% damping ratio in modes 1 and 4 results in almost the same response with the Caughey damping model for all the T_1 / T_p values and all response parameters.

Table 3. Caughey and Rayleigh damping comparison.

Mode	Mode 1 damping (%)	Mode 2 damping (%)	Mode 3 damping (%)	Mode 4 damping (%)
Caughey 2% in modes 1 through 6	2.00	2.00	2.00	2.00
Rayleigh 2% in modes 1 and 2	2.00	2.00	4.98	9.65
Rayleigh 2% in modes 1 and 4	2.00	0.65	1.10	2.00

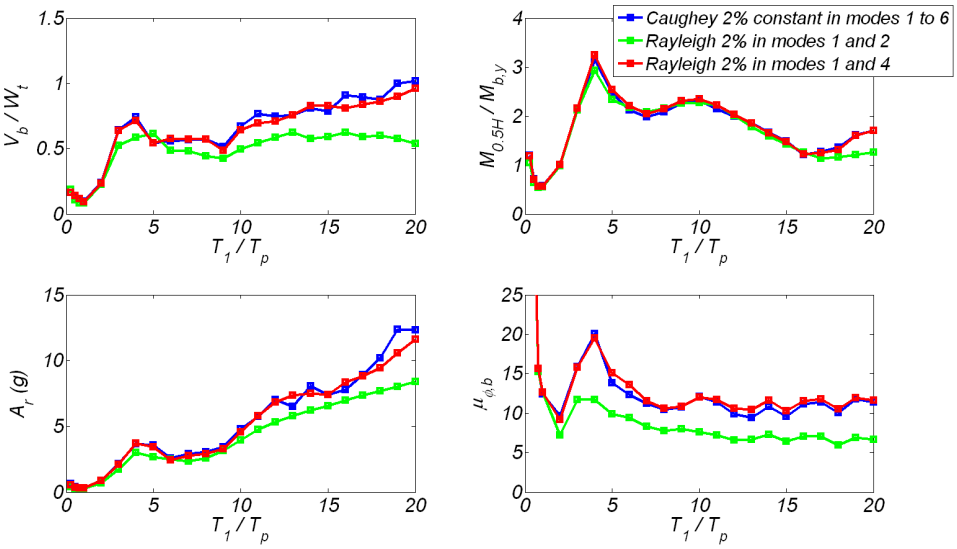

Figure 24. Damping sensitivity study for the 20-story building for pulse B and R = 4.

A MODIFIED MODAL RESPONSE SPECTRUM ANALYSIS METHOD FOR RC CANTILEVER WALLS WITH BASE INELASTICITY

Independent of the number of stories for the three pulse types and R values considered, MRSA, using effective flexural rigidities, significantly underestimated different response quantities, when used a uniform R factor in all the first four modes, and the SRSS combination rule. For T_1 / T_p smaller than one corresponding to low-frequency excitation, the response was first mode dominated. In this excitation period range, MRSA did not account for the post-yield base section hardening of the walls, resulting in an underestimation of the response; in addition section hardening was excessive for R = 4 and 6. For T_1 / T_p larger or equal than one, MRSA using the SSRS combination method and a uniform R factor in all the four modes significantly underestimated the response for all pulses and R values, because inelastic response at the base of cantilever wall buildings does not reduce the second and higher modes as much as the first mode of response.

A modified modal response spectrum analysis (MMRSA) method is presented that considers only the first three modes of response and uses a yield reduction factor R_1, and R_H for the first and higher (second and third) modes, respectively. Modal characteristics are computed using effective flexural rigidities. In this approach, the elastic response modal parameter Q^i (bending moment, shear force, floor acceleration) of interest at floor i can be computed as:

$$Q^i = \sqrt{\left[Q_1^i \cdot \frac{\Omega_{b,o}}{R_1}\right]^2 + \frac{\left[Q_2^i\right]^2 + \left[Q_3^i\right]^2}{\left(R_H\right)^2}} \tag{5}$$

where Q_q is the mode q elastic contribution to the response parameter considered. The base section overstrength factor $\Omega_{b,o}$ is the ratio of the peak expected base bending moment $M_{b,o}$ to $M_{b,y}$. Having determined the expected flexural yield strength of a wall, Equation 5 can be used to calculate floor accelerations and bending moments, above the base of the wall, and shear forces

along its entire height. Once $M_{b,y}$, and $M_{b,q}$ are known, factor R_1 is computed based on Equation 6.

$$R_1 = \frac{m_t \cdot H \cdot \sqrt{\sum_{q=1}^{4}\left[r_{M,q,b} \cdot Sa\left(T_q\right)\right]^2}}{M_{b,y}} \tag{6}$$

As defined above for the three buildings considered, the modal parameters $r_{M,i}$, $r_{V,i}$, $r_{A,i}$ and thus Q_q^i are known from modal analysis (see Figure 8). For the analysis using the close-form pulses, factor R_1 is equal to R used for the MRSA (compare Equations 4 and 6). Also peak values of $M_{0.5H}$, V_b, A_r, and $\Omega_{b,o}$ were computed with NDRHA. Here, Equation 5 can be solved separately for the peak values of $M_{0.5H}$, V_b, A_r, in terms of R_H. Figure 25 plots the results of R_H for the 20-story building with $EI_e = 0.4EI_g$ for all the three pulses and T_1 / T_p between 0.75 and 20. Figure 25 shows that for all three response quantities, all pulses, and all R factors, R_H was significantly smaller than R_1 and smaller than 2.0, except Pulse C for base shear force and T_1 / T_p = 8. In some cases, especially for T_1 / T_p between 0.75 and 4, values of R_H smaller than one are computed. In these cases even considering the second and third mode elastic underestimates the response.

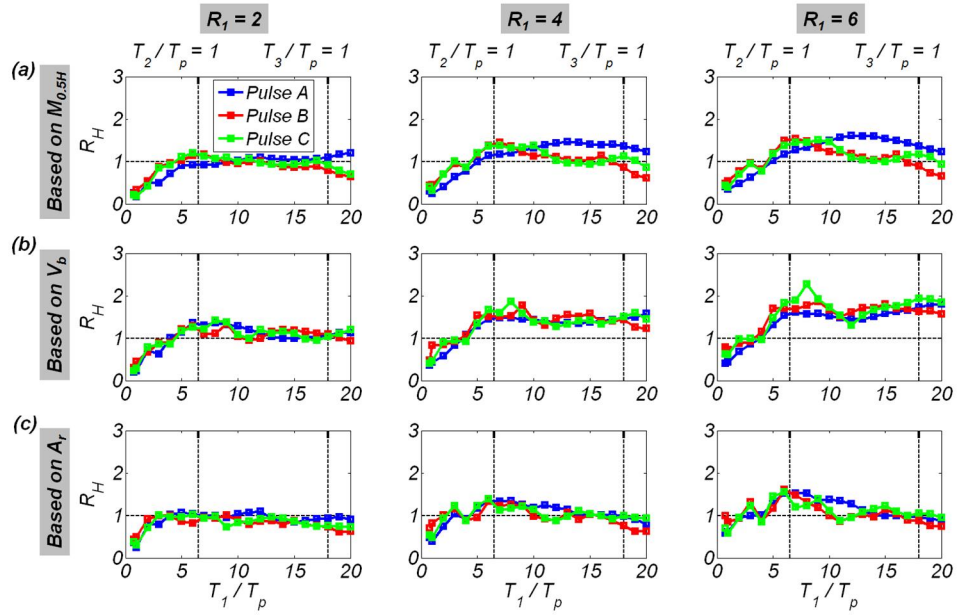

Figure 25. Yield reduction factor R_H for higher modes computed based on: (a) mid-height bending moment; (b) base shear force; and (c) roof acceleration obtained from NDRHA of the 20-story building.

Comparison of MRSA and the MMRSA results for the three buildings subjected to near-fault records is shown in Figure 10. Results of MRSA with a uniform R factor in the first four modes and MMRSA as described in Equations 5 and 6, using R_H = 1, are presented. For the JFA292, RRS228, and PCD164 records, the $R_1 = R$ factors computed using Equation 6 for the 10-, 20-,

and 40-story buildings are 5.97, 2.74, and 2.25, respectively. In all three cases, MRSA significantly underestimated the three response parameters along the height of the buildings. The MMRSA significantly improved the estimation of all response envelopes. The MMRSA significantly underestimated the floor accelerations at the bottom 25% of the height of the buildings. The total acceleration computed with modal response spectrum analysis, independent of the *R* values used, results in zero acceleration at the base of the fixed-base buildings.

SUMMARY AND CONCLUSIONS

This report investigated the inelastic response of tall cantilever wall buildings subjected to pulse-type ground motion, emphasizing the relationship between ground motion characteristics and higher modes of response, especially the second and third mode. Three 10-, 20-, and 40-story high cantilever wall buildings were designed to develop all nonlinear deformations at a flexural plastic hinge region located at their base. Nonlinear dynamic response history analyses (NDRHA) of these buildings was carried out. Initially, each building was subjected to both a near-fault record and a representation of this record using a close-form pulse. Then, an extensive parametric analytical study was conducted for each building subjected to three close-form pulses. Twenty three distinct pulse periods and three pulse amplitudes at each period were considered to study different levels of inelastic response. The following conclusions were drawn:

1. Strong pulse-type ground motions with the predominant pulse period in the range of the second structural modal period computed with effective flexural rigidities significantly excited the first, and second mode, causing highly inelastic response at the base of the walls for all buildings considered.
2. Simple close-form pulses provided fair approximations of the distinct pulses contained in near-fault records. Using the pulse approximations, the computed response in terms of section bending moment, shear force, and floor acceleration were similar to the corresponding response computed using near-fault records.
3. Strong pulse-type motion with a predominant pulse period close to or shorter than the second modal period excited significantly the second mode of response and resulted in bending moment demands at the intermediate wall height that far exceeded the base bending moment yield strength. Designing these regions to remain elastic requires large to excessive amounts of longitudinal reinforcement.
4. For any T_1 / T_p greater than one, the peak shear force at 75% of the height of the buildings, $V_{0.75H}$, approached or even exceeded 50% of the peak base shear force. For $T_1 / T_p = 3$, for all three pulses, $V_{0.75H}$ approached or even exceeded the peak base shear force.
5. Inelastic response at the base of cantilever wall buildings did not reduce the second and higher modes as much as the first mode of response.
6. Using a uniform yield reduction factor *R* in all the modes and the SRSS combination method, modal response spectrum analysis significantly underestimated the bending moments, shear forces, and floor accelerations along the height of the buildings for T_1 / T_p greater than one.
7. This underestimation increased with increasing *R* and with an increase of T_1 / T_p between 1 and 4. The level of underestimation was independent of the number of stories and showed small sensitivity to the pulse type and to the response parameter.
8. Modified modal response spectrum analysis that considered a yield reduction factor R_H factor in the second and higher modes equal to one (or much smaller than this used for the first

mode), significantly improved the estimation of forces and accelerations along the height of cantilever wall buildings.

REFERENCES

1. Blakeley RWG, Cooney RC, Megget LM. Seismic shear loading at flexural capacity in cantilever wall structures. *Bulletin New Zealand National Society Earthquake Engineering* 1975; 8: 278–290.
2. Derecho AT, Iqbal M, Ghosh SK, Fintel M, Corley WG, Scanlon A. *Structural Walls in Earthquake-Resistant Buildings Dynamic Analysis of Isolated Structural Walls Development of Design Procedure – Design Force Levels*. Portland Cement Association, 1981.
3. Eibl J, Keintzel F. Seismic shear forces in RC cantilever shear walls. *Proceedings, 9th World Conference on Earthquake Engineering*, Tokyo/Kyoto, Japan 1988, Report 9-1-1.
4. Paulay T, Priestley MJN. *Seismic Design of Reinforced Concrete and Masonry Buildings*. Wiley: Hoboken, NJ, 1992.
5. Eberhard MO, Sozen MA. Member behavior-based method to determine design shear in earthquake-resistant walls. *Journal of Structural Engineering* 1993; 119(2):619–640.
6. Filiatrault A, D'Aronco D, Tinawi R. Seismic shear demand of ductile cantilever walls: a Canadian code perspective. *Canadian Journal of Civil Engineering* 1994; 21:363–376.
7. Panneton M, Léger P, Tremblay R. Inelastic analysis of a reinforced concrete shear wall building according to the National Building Code of Canada 2005. *Canadian Journal of Civil Engineering* 2006; 33:854-871.
8. Rutenberg A, Nsieri E. The seismic shear demand in ductile cantilever wall systems and the EC8 provisions. *Bulletin of Earthquake Engineering* 2006; 4:1–21.
9. Moehle JP, Sozen MA. Experiments to study earthquake response of R/C structures with stiffness interruptions (4th Ed.). *Civil Engineering Studies, Structural Research Studies No. 482*, University of Illinois, Urbana-Champaign, 1980.
10. Panagiotou, M., Restrepo, J.I., and Conte J.P. Shake Table Test of a 7-Story Full Scale Reinforced Concrete Wall Building Slice, Phase I: Rectangular Wall. *ASCE Journal of Structural Engineering*, Vol. 137, No. 6, 2011.
11. Panagiotou M. Seismic design, testing, and analysis of reinforced concrete wall buildings. Ph.D. Thesis, University of California, San Diego, 2008.
12. Park R, Paulay T. *Reinforced Concrete Structures*. John Wiley & Sons, Inc., NJ, 1975.
13. ACI 318-08. *Building Code Requirements for Structural Concrete (ACI 318-08) and Commentary*. ACI Committee 318, Farmington Hills, 2008.
14. ASCE 7-05. *Minimum Design Loads for Buildings and Other Structures*. American Society of Civil Engineers, 2006.
15. CEN EC8: *Design of Structures for Earthquake Resistance*. European Committee for Standardisation: Brussels, Belgium, 2004.
16. NZS 3101. *New Zealand Standard, Part 1- The Design of Concrete Structures*, Standards New Zealand, Wellington, New Zealand, 2006.
17. CSA Standard A23.3-04. Design of Concrete Structures. *Canadian Standard Association*, Rexdale, Canada. 2005; 214pp.
18. Moehle J, Bozorgnia Y, Yang TY. The Tall Buildings Initiative. *Proceedings SEAOC Convention*. 2007; 315-324.

19. Priestley MJN, Calvi GM, Kowalsky MJ. *Displacement Based Seismic Design of Structures*. IUSS Press, Pavia, Italy. 2007.
20. Panagiotou M, Restrepo JI. Dual-plastic hinge design concept for reducing higher-mode effects on high-rise cantilever wall buildings, Vol. 38, Issue 12, pp 1359-1380, 2009.
21. Sullivan TJ, Priestley MJN, Calvi GM, Estimating the Higher-Mode Response of Ductile Structures. *Journal of Earthquake Engineering*, 2008; 12(4):456-472
22. Rodríguez ME, Restrepo JI, Carr AJ. Earthquake-induced floor horizontal accelerations in buildings. *Earthquake Engineering and Structural Dynamics* 2002; 31:693-718.
23. Goel RK, Chopra AK. Role of higher-"mode" pushover analyses in seismic analysis of buildings. *Earthquake Spectra* 2005; 21(4):1027-1041.
24. Chopra AK, Goel RK, Chintanapakdee R. Evaluation of a Modified MPA Procedure Assuming Higher Modes as Elastic to Estimate Seismic Demands. *Earthquake Spectra* 2004; 20(3):757–778.
25. Bertero VV, Mahin SA, Herrera RA. Aseismic design implications of San Fernando earthquake records. *Earthquake Engineering and Structural Dynamics* 1978; 6(1):31-42.
26. Anderson JC, Bertero VV, Uncertainties in Establishing Design Earthquakes. *ASCE Journal of Structural Engineering 1987*; Vol. 113; No. 8; 1709-1724.
27. Alavi B, Krawinkler H. Behavior of moment-resisting frame structures subjected to near-fault ground motions. *Earthquake Engineering and Structural Dynamics* 2004; 33:687–706.
28. Kalkan E, Kunnath SK. Effects of fling step and forward directivity on seismic response of buildings. *Earthquake Spectra* 2006; 22(2):367-390.
29. Krishnan S. Case studies of damage to 19-storey irregular steel moment-frame buildings under near-source ground motion. *Earthquake Engineering and Structural Dynamics* 2007; 36:861–885.
30. Dicleli M, Mehta A. Effect of near-fault ground motion and damper characteristics on the seismic performance of chevron braced steel frames. *Earthquake Engineering and Structural Dynamics* 2007; 36:927-948.
31. Hall JF, Heaton TH, Halling MW, Wald DJ. Near source ground motion and its effects on flexible buildings. *Earthquake Spectra* 1995; 11:569–606.
32. Akkar S, Yazgan U, Gulkan P. Drift estimates in frame buildings subjected to near-fault ground motions. *Journal of Structural Engineering* 2005; 131(7):1014-1024.
33. Liao W-I, Loh C-H, Wan S. Earthquake responses of RC moment frames subjected to near-fault ground motions. *Structural Design of Tall Buildings* 2001; 10:219-229.
34. Panagiotou M, Calugaru V, Visnjic T. Higher mode effects on the seismic response of tall cantilever wall buildings subjected to near fault ground motions. *Proceedings, Structural Engineers Association of California Convention*, San Diego, CA 2009; 345–357.
35. Somerville PG, Smith NF, Graves RW, Abrahamson NA. Modification of empirical strong ground motion attenuation relations to include the amplitude and duration effects of rupture directivity. *Seismological Research Letters* 1997; 68:199-222.
36. Iwan WD, Huang CT, Guyader AC. Evaluation of the effects of near-source ground motions. *Final Report on Research Conducted under PEER/PGE Research Program*, California Institute of Technology, 1998.
37. Sasani M, Bertero VV. Importance of severe pulse-type ground motions in performance-based engineering: historical and critical review. *Proceedings, 12th World Conference on Earthquake Engineering* 2000, Report No. 1302.

38. Makris N, Black JC. Dimensional analysis of bilinear oscillators under pulse-type excitations. *Journal of Engineering* Mechanics 2004; 130(9): 1019-1031.
39. Malhotra PK. Response of buildings to near-field pulse-like ground motions. *Earthquake Engineering and Structural Dynamics* 1999; 28:1309-1326.
40. MacRae GA, Morrow DV, Roeder CW. Near-fault ground motion effects on simple structures. *Journal of Structural Engineering* 2001; 127:996–1004.
41. Cuesta I, Aschheim MA. Isoductile strengths and strength reduction factors of elasto-plastic SDOF systems subjected to simple waveforms. *Earthquake Engineering and Structural Dynamics* 2001; 30:1043–1059.
42. Mylonakis G, Reinhorn AM. Yielding oscillator under triangular ground acceleration pulse. *Journal of Earthquake Engineering* 2001; 5:225–251.
43. Mavroeidis GP, Papageorgiou AS. A mathematical representation of near-fault ground motions. *Bulletin of the Seismological Society of America*, June 2003; 93(3):1099-1131.
44. Baker JW. Quantitative classification of near-fault ground motions using wavelet analysis. *Bulletin of the Seismological Society of America*, October 2007; 97(5):1486-1501.
45. Carr AJ. *Ruaumoko – A Program for Inelastic Time-History Analysis*. Department of Civil Engineering, University of Canterbury, New Zealand, 1998.
46. Chopra AK. *Dynamics of Structures: Theory and Applications to Earthquake Engineering*. Prentice Hall: Englewood Cliffs, NJ, 2001.